

Cite this: *J. Mater. Chem. B*, 2018,  
6, 4645

# Self-assembled proteinaceous wound dressings attenuate secondary trauma and improve wound healing *in vivo*<sup>†</sup>

Jian Zhao,<sup>‡a</sup> Yangcui Qu,<sup>‡b</sup> Hong Chen,<sup>Ⓜb</sup> Rui Xu,<sup>\*c</sup> Qian Yu<sup>Ⓜ\*b</sup> and Peng Yang<sup>Ⓜ\*a</sup>

A new type of wound dressing that can be easily peeled from a wound during frequent changes is essential in clinical applications to reduce secondary trauma and relieve the pain suffered by patients. Here, we discover that a phase-transitioned lysozyme nanofilm (PTLF) composed of self-assembled protein nanoparticles with an amyloid-like internal structure can be disassembled and detached from a substrate surface under the stimulus of vitamin C solution. Accordingly, stimuli-responsive gauze coated with this phase-transitioned lysozyme nanofilm (PTLF@gauze) was developed. This novel wound dressing, PTLF@gauze, was fabricated through a simple, universal and environmentally benign approach by immersing pristine gauze in the lysozyme phase transition aqueous solution for minutes. In comparison with pristine gauze, the PTLF@gauze can be peeled from a mouse wound with less strength, causing less secondary trauma. This is due to the disassembly and detachment of the PTLF from the gauze in the presence of vitamin C, which is entirely different from normal low-adherent wound dressings based on anti-fouling. Additionally, the PTLF@gauze was shown to accelerate wound closure using a murine wound healing model owing to the anti-infection properties of PTLF. This work thus provides an effective surface modification method for medical devices and suggests the great potential applications of self-assembled proteinaceous coatings in wound care.

Received 26th April 2018,  
Accepted 14th June 2018

DOI: 10.1039/c8tb01100a

rsc.li/materials-b

## 1. Introduction

The skin is the largest organ in the human body and plays important roles in continuously maintaining life. When the skin is injured, it is essential to cover the wound with a dressing to prevent the wound from bacterial infection and massive loss of tissue fluid, in order to facilitate wound closure and reduce scab formation.<sup>1–4</sup> Cotton gauze as a wound dressing has been used for a long time and is still widely used to date because of its ease of use, ready accessibility, lower treatment costs, and better patient acceptance.<sup>5</sup> However, a major drawback in

traditional dressing materials is the adherence between the gauze and the damaged tissue. If separation of gauze and the wound is difficult during a dressing change, secondary damage to the wound will occur and prolong the wound healing time, especially in the treatment of chronic wounds.<sup>6</sup> It is reported that in the United States, an estimated 6.5 million people suffer from chronic skin ulcers while 1.25 million suffer from burns, giving rise to an annual healthcare bill of around \$25 billion.<sup>7,8</sup> A wound dressing with the ability to be easily stripped off is therefore highly desirable in order to help lighten the pain suffered by patients during frequent dressing changes and to accelerate wound healing. Recently, zwitterionic hydrogel dressings<sup>9–12</sup> and hydrophilic polymer grafted fabric dressings<sup>6,13–17</sup> with anti-fouling functions have been developed to deal with this issue. However, the mechanical properties of hydrogel dressings are often poor, and it is thereby difficult to store and handle in clinical practice. On the other hand, although surface grafted polymer brushes have been extensively explored to fabricate anti-fouling surfaces on fabric dressings, the common grafting approaches require complex molecular design and chemical synthesis, *e.g.* surface-initiated atom transfer radical polymerization (ATRP), which is sensitive to oxygen and requires a large amount of costly and harmful transition-metal complex catalyst.<sup>16,17</sup>

<sup>a</sup> Key Laboratory of Applied Surface and Colloid Chemistry, Ministry of Education, School of Chemistry and Chemical Engineering, Shaanxi Normal University, Xi'an 710119, China. E-mail: yangpeng@snnu.edu.cn

<sup>b</sup> State and Local Joint Engineering Laboratory for Novel Functional Polymeric Materials, College of Chemistry, Chemical Engineering and Materials Science, Soochow University, 199 Ren'ai Road, Suzhou, 215123, P. R. China. E-mail: yuqian@suda.edu.cn

<sup>c</sup> Department of Neurology, Xinqiao Hospital and The Second Affiliated Hospital, Army Medical University (Third Military Medical University), 183 Xinqiao Zhengjie, Shapingba District, Chongqing 400037, China. E-mail: xuruiwade1@sina.com

<sup>†</sup> Electronic supplementary information (ESI) available. See DOI: 10.1039/c8tb01100a

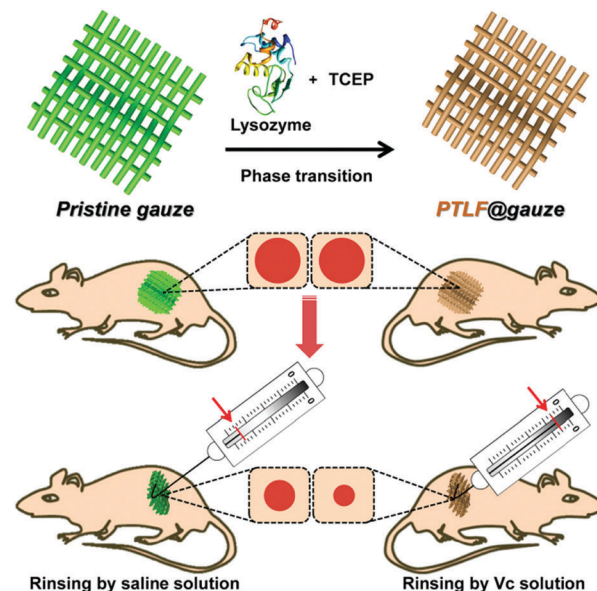
<sup>‡</sup> These authors contributed equally to this work.

Therefore, it is critical to develop a simple, universal and environmentally benign method, which does not require complex chemical synthesis, for the preparation of a robust wound dressing that can be easily peeled from a wound at daily intervals for changes, causing less secondary damage and promoting wound healing.

As the essential constituent of organisms, natural peptides or proteins generally exhibit excellent biocompatibility. Inspired by self-assembled peptide or protein amyloid structures, a number of remarkable self-assembling biomaterials have been developed.<sup>18–21</sup> In our previous work, we found that lysozymes could undergo a fast phase transition process in a few minutes with a disulfide breaker, tris(2-carboxyethyl)phosphine (TCEP), in an aqueous solution.<sup>22</sup> During the phase transition process, the partially unfolded monomers aggregated to form amyloid-like protein nanoparticles that further hierarchically assembled into a 2D nanofilm at the air/water or water/solid interface and a network consisting of microparticle-aggregated necklace-like fibers in the bulk solution, respectively.<sup>23,24</sup> It was also reported that this phase transition process depended on the concentration of lysozyme solution, and that phase transition would not occur when the concentration of the lysozyme solution was lower than  $0.05 \text{ mg ml}^{-1}$  under TCEP (1.0 mM, pH 6.5).<sup>24</sup> The 2D phase-transitioned lysozyme nanofilm (PTLF) could stably adhere onto virtually arbitrary substrate surfaces to form a robust and conformal coating and biomineralization platform, and show low cytotoxicity, blood compatibility and durable *in vitro* and *in vivo* broad-spectrum antimicrobial efficacy against Gram-positive/negative bacteria and fungi.<sup>24–27</sup> Even though a variety of functional materials based on amyloid-like assemblies have been developed, the effort to eliminate or inhibit amyloids *in vivo* is ongoing since such a breakthrough may impart the amyloid-based material systems with novel stimuli-responsiveness and other necessary features required for biomedicines.<sup>28</sup> In this regard, vitamin C (Vc), which is abundant in citrus fruits and vegetables, has potential therapeutic roles for neurodegenerative diseases owing to its abilities in amyloid structure degradation and the amelioration of aggregated amyloid plaques in animal models.<sup>29–34</sup> Accordingly, we speculate that a self-assembled lysozyme nanofilm with an amyloid-like internal structure (PTLF) could be degraded in the presence of Vc and detached from the substrate surface. Consequently, traditional wound dressings, such as cotton gauze, coated with this nanofilm may be excellent candidates for promoting wound healing and helping to lighten the pain suffered by patients during frequent dressing changes (Scheme 1).

## 2. Results and discussion

Lysozyme solution is able to undergo super-fast phase transition when mixed with TCEP solution, and this novel process has been investigated thoroughly in our previous work.<sup>35</sup> During the phase transition process, the mixed solution gradually turned turbid and exhibited an enhanced Tyndall effect, the scattering of light as a light beam passes through colloids (Fig. 1A), implying a stepwise increase in the colloidal particle size in the mixture; however,



Scheme 1 A schematic illustration of the fabrication of PTLF@gauze and the differences in peeling strength and wound healing between pristine gauze and PTLF@gauze.

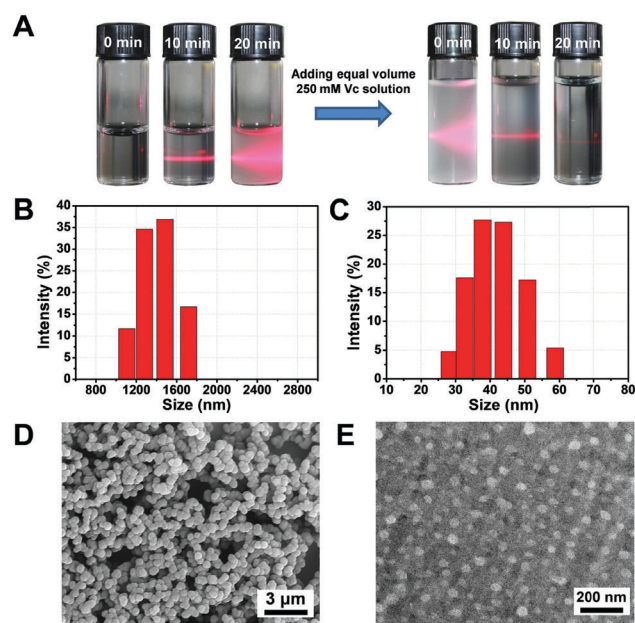


Fig. 1 Characterization of the effect of Vc on the phase-transitioned product in bulk solution. (A) Changes in solution transparency and light scattering during the phase transition and disassembly processes in 250 mM Vc solution, respectively; (B and C) the particle size distribution of the PTL product before (B) and after (C) incubation with 250 mM Vc solution for 20 minutes, measured by DLS; (D) a SEM image of the PTL product; (E) a TEM image of the PTL product after incubation with 250 mM Vc solution for 20 minutes. The mixture was dialyzed before TEM characterization. The phase transition process in the above experiments occurred with  $2 \text{ mg mL}^{-1}$  of lysozyme and 50 mM of TCEP (pH 7.2).

the micro-aggregates formed by phase transition could not be stably suspended in the solution for a long time, and the aggregates precipitate from the solution slowly due to gravity (Fig. S1, ESI†).

When an equal volume of 250 mM Vc solution was added into the mixture, it was interesting to observe that the solution returned to be transparent and the degree of light scattering decreased gradually within a few minutes, possibly resulting from the reduction of particle size. In order to verify this judgment, the particle size distribution in the mixture was characterized using dynamic light scattering (DLS). As shown in Fig. 1B, there were large aggregates with sizes between 1000–1800 nm in the mixture, and the size reduced to 30–60 nm after incubation with Vc solution for 20 minutes (Fig. 1C). For the DLS measurements, the phase-transitioned lysozyme solution was diluted 50 times using pure water, which indeed suggested that simple dilution with pure water would not disassemble the large aggregates into small particles. The morphology of the particles in the phase transition product was observed using scanning electron microscopy (SEM) by dropping the turbid phase-transitioned lysozyme solution on a Si wafer surface. It is shown in Fig. 1D and Fig. S1 (ESI<sup>†</sup>) that the product formed in the bulk solution at 20 minutes and the precipitation at 5 hours both contained an aggregation of spherical particles with sizes of  $\sim 500$  nm. This result indicates that in the absence of Vc, the aggregation existed stably without further decomposition or disassembly over a prolonged storage period. As revealed by transmission electron microscopy (TEM) in Fig. 1E and atomic force microscopy (AFM) in Fig. S2 (ESI<sup>†</sup>), these large supra-molecular assemblies disassembled into small particles with irregular boundaries after the addition of Vc solution.

Due to the similarities between the PTL product in bulk solution and the PTLF at the solid/water interface in terms of the supramolecular self-assembled structure,<sup>23,24</sup> it is rational to consider that the PTLF coated on the substrate surface could also disassemble into small parts in the presence of Vc. To further investigate the effect of Vc on the PTLF, an Au wafer was chosen as the substrate and the PTLF was formed on the surface by simply immersing the substrate in a lysozyme phase transition solution. The morphology of the PTLF was characterized using AFM. As shown in Fig. 2A, the original PTLF was actually composed of densely aggregated nanoparticles, which

formed robust adhesion with the substrate surface<sup>24</sup> through a multiplex interfacial bonding model.<sup>36</sup> After the substrate was partially immersed in 500 mM Vc solution for 20 minutes at room temperature, it was clearly observed that the PTLF detached from the area which was immersed in Vc solution (Fig. S3, ESI<sup>†</sup>). Additionally, the AFM image also implies the absence of densely aggregated large nanoparticles in this area (Fig. 2A). The water contact angles (WCAs) of the different Au wafer surfaces are shown in Fig. 2B. It was observed that the WCA decreased from  $75 \pm 6^\circ$  for pristine Au to  $54 \pm 3^\circ$  for PTLF coated Au, and there was almost no difference between the WCA of PTLF coated Au before ( $54 \pm 3^\circ$ ) and after ( $58 \pm 4^\circ$ ) being immersed in Vc solution. The characterization of the ellipsometry showed that the PTLF coating thickness on the Au wafer surface decreased from  $56.8 \pm 1.5$  nm (before Vc) to  $5.9 \pm 0.3$  nm (after Vc). These results suggested that there was still a thin PTLF layer attached to the immersed area after Vc-induced detachment, which was also supported by X-ray photoelectron spectroscopy (XPS) (Fig. S4, ESI<sup>†</sup>) and energy dispersive X-ray spectroscopy (EDS) (Fig. S5, ESI<sup>†</sup>) analysis. Compared to the Au substrate, the PTLF adhered onto the Si substrate showed similar detachment behavior with the addition of Vc solution (Fig. S6, ESI<sup>†</sup>). The stacked nanoparticles containing amyloid-like molecular stacking in the nanofilm exhibited hydrophobic Trp blocks and polar carboxyl, amine, amide, hydroxyl and thiol groups as well as certain positive charges on their surface, resulting in combinational interfacial adhesion with a given substrate.<sup>36</sup> Therefore, a thin part of the PTLF that directly interacted with the substrate may not be detached in the presence of Vc. Furthermore, it was found in our previous work that the disassembly of PTLFs accelerated with increasing Vc concentration<sup>37</sup> and the optimal concentration of Vc was closely dependent on the experimental and application purposes.

For further insight into the disassembly process of the PTL product, changes in lysozyme molecular weight and conformation during the process were investigated. Firstly, changes in protein primary structure were measured using sodium dodecyl sulphate polyacrylamide gel electrophoresis (SDS-PAGE), which separates proteins according to their molecular weight. As shown in Fig. 3A, there was no change in the molecular weight between the PTL product and the disassembled PTL product, implying that disassembly is not attributed to the backbone degradation of protein molecules. Additionally, it is necessary to study the evolution of the secondary structure and hydrophobicity of the protein upon incubation with Vc. The lysozyme fast phase transition in the presence of TCEP involves protein unfolding, hydrophobicity-induced aggregation and the assembly of nanoparticles containing amyloid-like stacking structures.<sup>22–24</sup> In this process, the CD spectra of the PTL product exhibited the typical profile of anti-parallel  $\beta$ -sheet conformation at 216 nm (Fig. 3B).<sup>38</sup> Upon incubation with 10 mM Vc, we observed a decrease in the  $\beta$ -sheet structure and an increase in random coil conformation (Fig. 3B). This result was also supported by Thioflavin T (ThT) staining, which is widely utilized to recognize the  $\beta$ -sheet-rich structures of amyloid (Fig. 3C).<sup>39</sup> The enhanced fluorescent intensity at 484 nm after ThT staining indicated the

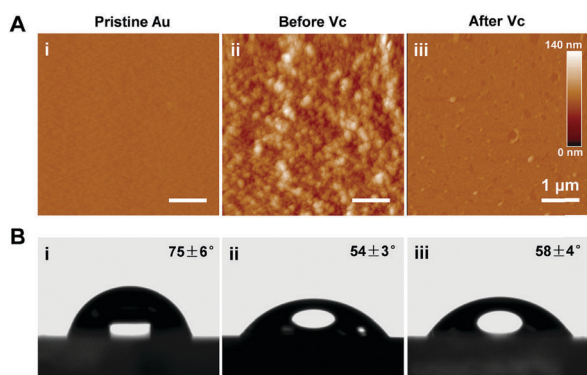
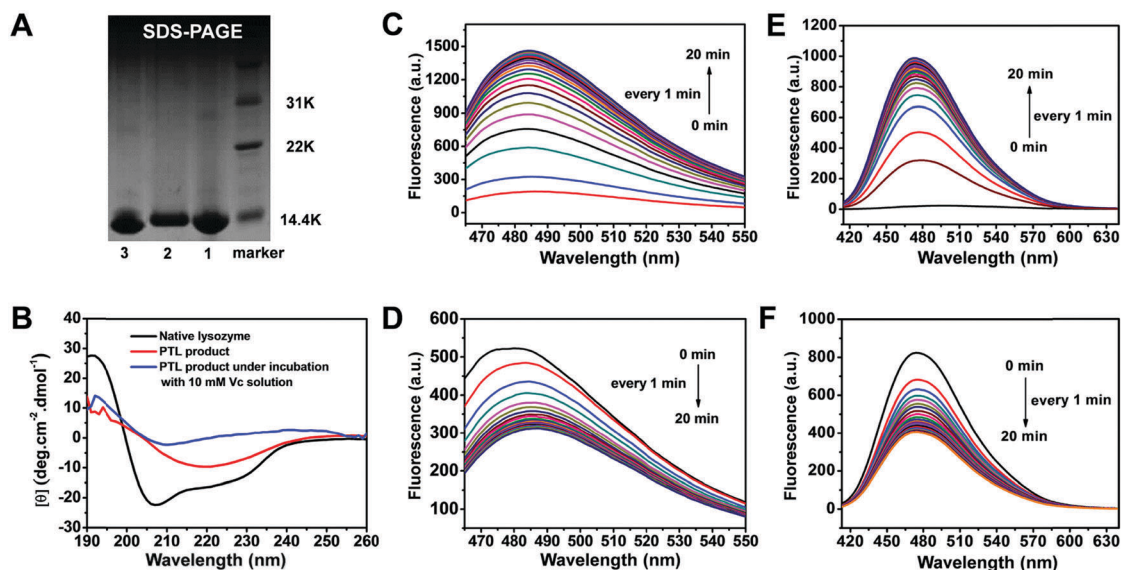


Fig. 2 Characterization of the effect of Vc on PTLFs. AFM images (A) and WCA images (B) of the pristine Au wafer surface (i) and the PTLF coated Au wafer surface before (ii) and after (iii) being immersed in 500 mM Vc solution. The PTLFs in these cases were prepared with 2 mg mL<sup>-1</sup> of lysozyme and 50 mM of TCEP (pH 7.2).



**Fig. 3** Characterization of the changes in lysozyme molecular weight, conformation and surface hydrophobicity during the phase transition and the PTL product disassembly processes. (A) SDS-PAGE image showing the PTL product (lane 1), the PTL product under incubation with 250 mM Vc solution (lane 2) and native lysozyme (lane 3). (B) Far-UV CD spectra of the native lysozyme, PTL product and disassembled PTL product (incubated with 10 mM Vc solution for 42 hours, this low concentration of Vc solution was used to avoid the interference of high concentration Vc on the far-UV CD spectra); the fluorescence spectra of the mixture at different phase transition times after staining with ThT (C) and ANS (E); 20 minutes later, an equal volume of 250 mM Vc solution was added to the mixture and the fluorescence spectra at different disassembly times were recorded (D and F). The phase transition process in the above experiments was performed with 2 mg mL<sup>-1</sup> of lysozyme and 50 mM of TCEP (pH 7.2).

formation of  $\beta$ -sheet structures during the phase transition process and this intensity attenuated gradually after the addition of 250 mM Vc solution (Fig. 3D). The effect of Vc on the surface hydrophobicity of the PTL product was further examined using anilino-1-naphthalene sulfonate (ANS) fluorescence emission, which is a commonly used approach to characterize protein folding intermediate states and to detect the presence of hydrophobic residues on the surfaces of proteins/amyloids.<sup>40</sup> Under reaction with TCEP, the hydrophobic residues of the lysozymes were rapidly exposed into the solution environment and the subsequent interaction of ANS with these exposed hydrophobic residues led to a significant increase in fluorescent intensity at 480 nm (Fig. 3E). After 20 minutes, 250 mM Vc solution was added into the mixture, and a decrease in ANS fluorescent intensity was observed (Fig. 3F), indicating less exposure of the hydrophobic residues to the solvent. According to our previous work, the PTL expresses obvious positive zeta potential under neutral or acidic pH conditions because of the isoelectric point (PI) of 11 for lysozymes.<sup>24</sup> Vc, as an acidic molecule, tends to transform into ascorbate anions in aqueous solution,<sup>41</sup> so the hydrophobic residues of the PTL product could be shielded by Vc molecules through an electrostatic interaction between negative ascorbate anions and the positive PTL product. The mechanism of Vc-induced disassembly of amyloid assemblies has been thoroughly studied in previous literature,<sup>34,42–45</sup> which has indicated the possible role of electrostatic interactions on amyloid fibril disassembly. These reports have also indicated that the disassembly of amyloid fibrils was not merely driven by electrostatic interactions, and other co-factors also made important contributions to the disassembly. For instance,

the hydrogen bonding between the -OH groups in Vc molecules and the exposed hydrogen atoms of the N-H groups in the  $\beta$ -sheet backbone of amyloids could interrupt the hydrogen bonding between  $\beta$ -sheets to destabilize the amyloid structure (Fig. S7, ESI†).<sup>34,45</sup>

Our previous work has demonstrated that the PTLF exhibits good biocompatibility and low cytotoxicity,<sup>22,26,27</sup> and further, based on the Vc-induced disassembly of PTLF, it is assumed that the PTLF holds great potential for the controllable release of biological matter in bioengineering (Fig. 4A). Albumin from bovine serum (BSA), *Escherichia coli* (*E. coli*), and the L929 cell line were chosen as a typical protein, bacteria, and cell to study release performance. The protein release ratio was determined by analyzing the image fluorescence intensity of BSA-fluorescein isothiocyanate (BSA-FITC) on the substrate, measured through fluorescence microscopy. The BSA-FITC expresses negative zeta potential under neutral or basic pH conditions,<sup>46</sup> so it can be adsorbed readily on the PTLF coated Au surface through electrostatic interactions. As a result, the fluorescence intensity of the PTLF coated Au surface was stronger than that of the pristine Au surface (Fig. 4B and Fig. S8, ESI†); in contrast, BSA-FITC could be released efficiently from the PTLF coated Au surface using simple Vc treatment, and the release ratio was up to 91.3%. Besides proteins, red fluorescent *E. coli* and L929 cells were also seeded and cultured on both pristine Au and PTLF coated Au surfaces respectively, and then incubated in 250 mM Vc solution for 20 minutes. The bacteria and cells were then observed under a fluorescence microscope and their numbers were counted in the fluorescence images. A slight increase in the bacteria and cells on the PTLF coated Au surface was observed

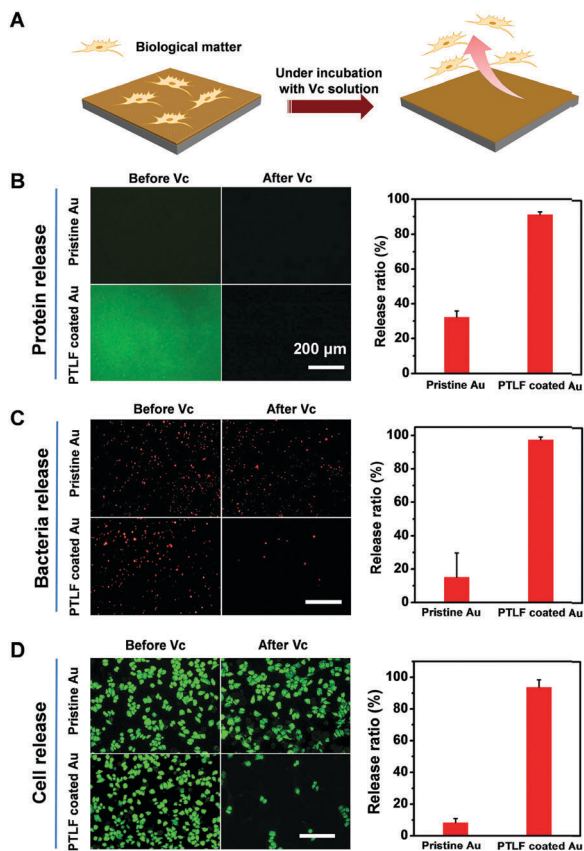


Fig. 4 (A) A schematic illustration of biological matter release from the PTLF coated substrate under incubation with Vc solution. Representative fluorescence images and the release ratios of proteins (B), bacteria (C), and cells (D) adhered on the pristine Au surface and the PTLF coated Au surface, before and after incubation with 250 mM Vc solution for 20 minutes. The release ratio of the proteins was determined using image fluorescence intensity. The numbers of bacteria and cells in the different groups were counted using IPP 6.0 software. The values were calculated as means  $\pm$  standard deviation ( $n = 5$ ). The PTLFs in these cases were prepared with 2 mg mL<sup>-1</sup> of lysozyme and 50 mM of TCEP (pH 6.2).

from Fig. 4C and D, which was possibly attributed to an increase in surface roughness after PTLF modification (Fig. 2). Few bacteria and cells were observed on the PTLF coated Au surface under incubation in Vc solution, and the release ratios were 97.5% and 93.7% respectively. In addition, as a control to suggest the key function of Vc for release, the release performance of protein, bacteria, or cells under treatment with PBS buffer was also characterized, and the corresponding release ratios were all just  $\sim 15\%$  (Fig. S9, ESI<sup>†</sup>), which was significantly lower than the values obtained in the Vc groups. Consequently, the PTLF can serve as a sacrificial layer to release adsorbed biological matter, which is entirely different from previous approaches.<sup>16,17</sup> It will be a facile and effective strategy to construct a smart surface with controllable adhesion.<sup>37,47–49</sup>

Cotton gauze is a commonly used wound dressing. Although it is very cheap and easy to handle clinically, it easily causes secondary trauma and pain to patients during frequent changes, because newborn cells and tissue adhere firmly to the gauze.<sup>17</sup> According to the above release results, the PTLF

modified gauze (PTLF@gauze) may be a good candidate to solve this problem. The PTLF@gauze was prepared through soaking pristine gauze in lysozyme phase transition solution for tens of minutes, followed by rinsing and drying. The initial WCA of the gauze increased from 0° (before) to 130  $\pm$  4° after the PTLF modification (Fig. 5A), demonstrating an effective coating on the gauze; this hydrophilicity change was possibly attributed to the exposure of lysozyme inner hydrophobic residues during the phase transition process. However, the WCA of the PTLF@gauze decreased gradually from 125  $\pm$  3° to 105  $\pm$  3° in 1 min and 0° in 2 min (Fig. 5A), reflecting the impregnation of water into the big internal voids of PTLF@gauze with time. The amount of droplet shrinking by water evaporation during this process is little, because the same water droplet on a flat Au wafer surface showed no remarkable decrease in droplet size in 2 min (Fig. S10, ESI<sup>†</sup>). Since water uptake and water vapor transmission rate (WVTR) are fundamental properties for a wound dressing to absorb the exudate and maintain the moist environment, it is necessary to characterize such properties for PTLF@gauze. As shown in Fig. 5B, the PTLF@gauze exhibited almost the same water uptake and WVTR as pristine gauze, because of the big internal void structure. The surface morphologies of different gauzes were observed through FESEM, and it was found from Fig. 5C that the surface of PTLF@gauze was entirely different from the pristine gauze, and due to the thin and homogeneous nanoscale thickness of PTLF, the intrinsic big internal void structure in the gauze was not blocked by the PTLF coating (Fig. S11, ESI<sup>†</sup>). Additionally, XPS and ATR-FTIR results obtained for the pristine gauze before and after PTLF modification were investigated. XPS analysis was conducted to assess elemental change on the gauze surface. As shown in Fig. 5D, a new peak corresponding to nitrogen element from lysozymes appeared in the spectrum of PTLF@gauze. The ATR-FTIR spectra are shown in Fig. S12 (ESI<sup>†</sup>), and the characteristic peaks of pristine gauze were located at 3320 and 1640 cm<sup>-1</sup>, which were attributed to O–H stretching vibrations and hemiacetal groups, respectively. Compared with pristine gauze, new absorption peaks corresponding to amide I (1540 cm<sup>-1</sup>) and amide II (1630 cm<sup>-1</sup> and 1660 cm<sup>-1</sup>) for the protein appeared in the spectrum of PTLF@gauze. Both the XPS and ATR-FTIR results demonstrated the successful proteinaceous modification on gauze through this protein phase transition process. Furthermore, the biocompatibility of the PTLF@gauze was characterized using a cytotoxicity evaluation. After fibroblasts were seeded on the samples for 3 days, it was clear to see under a fluorescence microscope that the GFP-fibroblasts could extend and adhere on to the surface of PTLF@gauze, and a typical spindle-like morphology for fibroblasts was observed (Fig. S13, ESI<sup>†</sup>). Cell numbers on the samples were counted by means of CCK8, and there were no significant differences between the blank control, pristine gauze, and PTLF@gauze (Fig. S13, ESI<sup>†</sup>). These results suggested that the PTLF@gauze exhibited good biocompatibility.

The strength required when the dressing was peeled from the mice wounds and the number of cells adhered on the dressings were then examined. Here, gauze Vc– or PTLF@gauze Vc– are

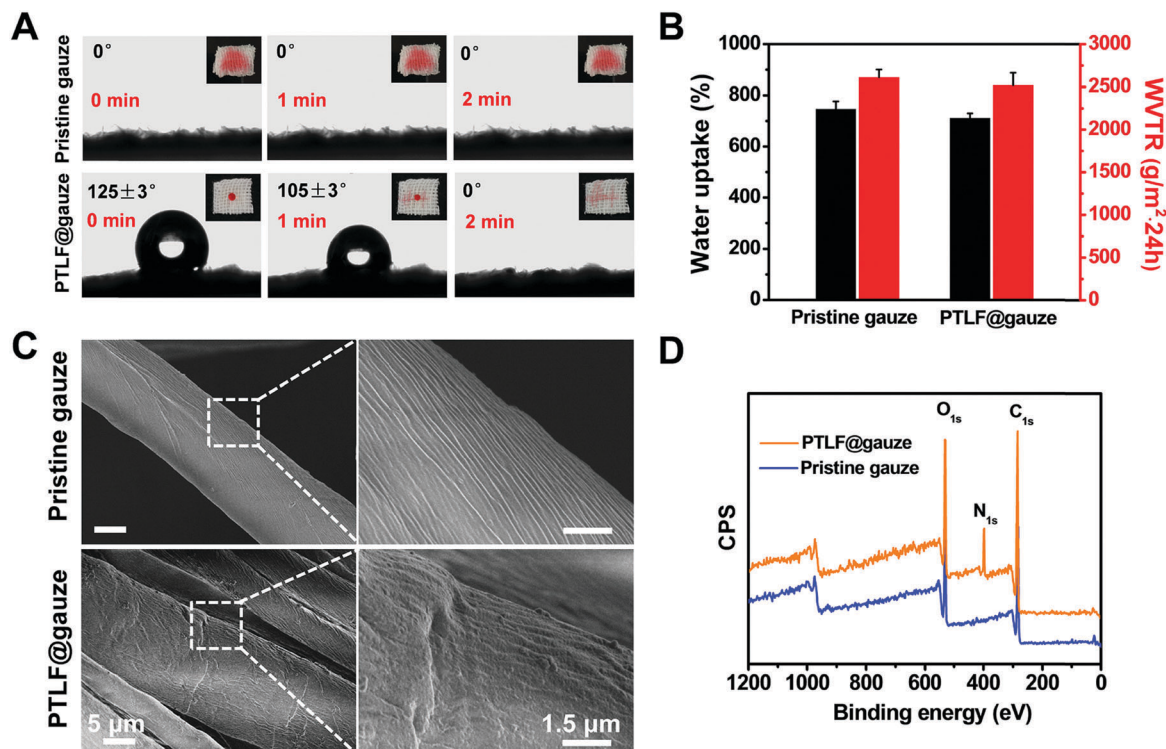


**Fig. 5** Characterization of PTLF@gauze. (A) Changes in water contact angles (with time) of the gauze before and after PTLF modification, the inserted small photos show the impregnation of Congo red water droplets into the gauze with time; (B) water uptake and water vapor transmission rate (WVTR) of the pristine gauze and PTLF@gauze; (C) FE-SEM images of the pristine gauze and PTLF@gauze, the right-hand images show partially enlarged detail; (D) XPS spectra of the pristine gauze (blue) and PTLF@gauze (orange). The PTLFs in these cases were prepared with 2 mg mL<sup>-1</sup> of lysozyme and 50 mM of TCEP (pH 7.2), and gauze and PTLF@gauze with eight layers were used.

abbreviations to indicate the pristine gauze or PTLF modified gauze treated with saline solution for one minute; gauze Vc+ or PTLF@gauze Vc+ are abbreviations to indicate the pristine gauze or PTLF modified gauze treated with 500 mM Vc solution for one minute before being peeled from the wound. As shown in Fig. 6A, the strength required to peel the dressing from the wounds was similar in the different groups at day 1. However at day 3, the average strengths for gauze Vc-, gauze Vc+, PTLF@gauze Vc- and PTLF@gauze Vc+ were  $0.56 \pm 0.05$  N,  $0.52 \pm 0.04$  N,  $0.46 \pm 0.07$  N and  $0.27 \pm 0.03$  N, respectively. The strength required for the PTLF@gauze Vc+ group was reduced by 51% compared to the control Vc- group (Fig. 6A and B), and the overall peeling processes of these two groups are displayed in Movie S1 (ESI<sup>†</sup>). Meanwhile, the cell adhesion on the peeled gauze in the different groups was characterized to evaluate wound secondary trauma during the peeling process. The fluorescence microscope photos (Fig. 6C) and the cell numbers (Fig. 6D) revealed that there were less adherent cells on the peeled gauze in the PTLF@gauze Vc+ group at day 3, demonstrating less damage to the wound. This is because the PTLF which adhered most cells had detached from the gauze surface under treatment with Vc solution. At day 1 post-wounding, the wound was liquid filled and there were not enough newborn cells and tissues on the wound, therefore the dressing could be detached from the wound easily, resulting in no significant differences in the strength and the adhered cell numbers among the four groups. At day 3, the dressing was adhered to

the wound tightly due to wound dehydration as well as the adhesion of newborn cells and tissue on the gauze, thus the dressings of gauze Vc-, gauze Vc+ and PTLF@gauze Vc- were hard to peel from the wound. However, the PTLF@gauze Vc+ dressing could be easily peeled from the wound (Fig. 6A and Movie S1, ESI<sup>†</sup>) and caused less damage to the wound (Fig. 6B and C), which was attributed to the detaching of PTLF from the gauze surface in the presence of Vc. Besides, *in vitro* experiments also indicated that the most adherent protein and bacteria on the PTLF@gauze surface could be released under treatment with Vc solution (Fig. S14, ESI<sup>†</sup>).

Another important function of wound dressings is to promote wound closure, so it is necessary to evaluate the effect of the PTLF coating on wound healing. Fig. 7A shows optical microscopic images of small wound cuts undressed (control group, left) or treated with pristine gauze or PTLF@gauze for 1, 3, 5 and 7 days. Bacterial infection symptoms such as excess exudate, suppuration, and scab formation were observed in the control and pristine gauze groups, while the wound in the PTLF@gauze group was neat without obvious infection symptoms. Meanwhile, the wound exudation was collected using a pipette and the number of bacteria in the exudation at day 1 and day 3 was determined by routine CFU analysis on an agar dish with different dilutions. Bacterial number analysis results shown in Fig. 7B demonstrated that the amount of bacteria in the PTLF@gauze group was observably less than

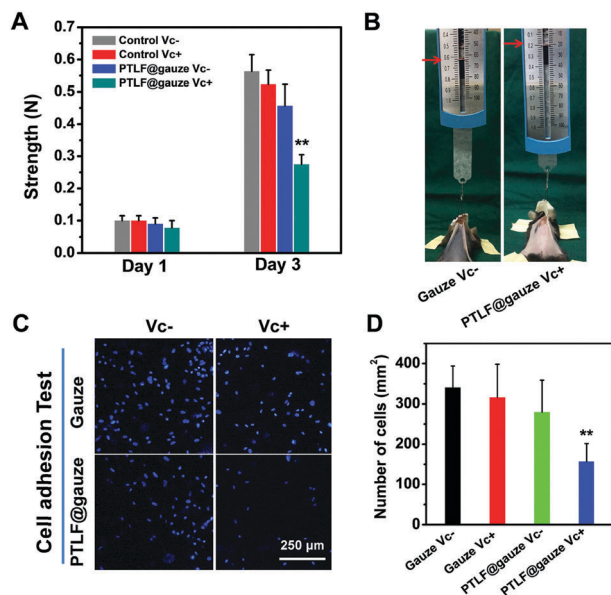


Fig. 6 Strength and cell adhesion tests. (A) The strength required to peel the dressing from the wound at day 1 and day 3 post-wounding; (B) photos to show the peeling of gauze Vc<sup>-</sup> and PTLF@gauze Vc<sup>+</sup> from the wound; (C) cells adhered to the dressing stained with 4',6-diamidino-2-phenylindole (DAPI) and (D) the numbers of cells in the different groups, counted using IPP 6.0 software. The values were calculated as means  $\pm$  standard deviation ( $n = 8$ ), \*\* $p < 0.01$ . The PTLFs in these cases were prepared with 2 mg mL<sup>-1</sup> of lysozyme and 50 mM of TCEP (pH 7.2), and gauze and PTLF@gauze with four layers were used.

that of the control and pristine gauze groups (a decrease of around 3 orders of magnitude at day 3). Moreover, the inflammatory response was assessed through CD206 (a marker of macrophages) and CCR7 (which plays an important role in the adaptive immune system) immunochemistry staining. The results in Fig. 7A indicate that the inflammatory response in the PTLF@gauze group was mild. This antibacterial capability is attributed to a synergistic combination of positive charge and hydrophobic amino acid residues enriched on polymeric aggregates in the PTLF.<sup>27</sup> It is well known that bacterial infection-induced inflammation leads to delayed wound healing,<sup>50–52</sup> so a variety of antibacterial dressings have been prepared to accelerate wound healing.<sup>3,7,10,11,53–55</sup> In this context, as the wound infection was controlled in the PTLF@gauze group, wound closure was then accelerated (Fig. 7A) and the statistical data (Fig. 7C) showed that the average area of the wound in the PTLF@gauze group at day 7 post-surgery was 0.0087 cm<sup>2</sup>, which was much less than that found in the control group (0.0462 cm<sup>2</sup>) or the pristine gauze group (0.0533 cm<sup>2</sup>). It was calculated that the wound healing ratio in these three groups was 94%, 68% and 70%, respectively. Additionally, we measured the length of the newly formed epithelium and the thickness of granulation tissue based on HE staining sections. At day 7, it was found that the wound treated with PTLF@gauze was almost closed with newly formed epithelium (Fig. 7A), and the average length of epithelial tongue was 641.5  $\mu$ m in the PTLF@gauze group, which was significant longer than that found in the control group or gauze group (Fig. 7D). Meanwhile, the granulation tissue was thickest when

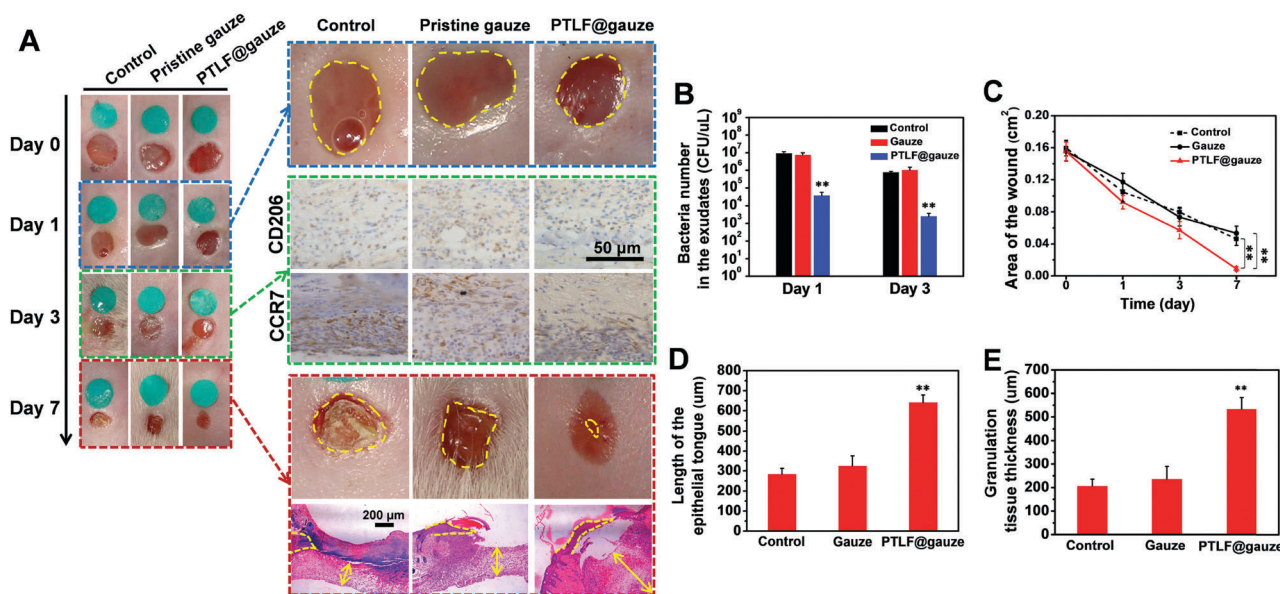


Fig. 7 Wound healing and *in vivo* anti-infection experiments. (A) The macroscopic appearance of the wounds post-surgery in the three groups at different time-points, CD206 and CCR7 immunochemistry staining in the wound tissue at day 3 post-surgery, and histological observation of the wound at day 7 post-surgery (the green disc is just a piece of green surgical glove and acts as a reference to qualitatively evaluate the size of the wound area); (B) number of bacteria in the exudates. The values were calculated as means  $\pm$  standard deviation ( $n = 3$ ), \*\* $p < 0.01$ ; (C) the area of the wound in the three groups at different time-points. The values were calculated as means  $\pm$  standard deviation ( $n = 3$ ), \*\* $p < 0.01$ ; (D) the average length of epithelial tongue and (E) the thickness of granulation tissue at day 7 post-surgery. The values were calculated as means  $\pm$  standard deviation ( $n = 3$ ), \*\* $p < 0.01$ . The PTLFs in these cases were prepared with 2 mg mL<sup>-1</sup> of lysozyme and 50 mM of TCEP (pH 7.2), and gauze and PTLF@gauze with eight layers were used.

the wound was covered with PTLF@gauze (Fig. 7E). It is thus demonstrated that the PTLF coating could effectively inhibit bacterial infection and accelerate wound healing.

### 3. Conclusion

In this work, we investigated the disassembly of the phase-transitioned lysozyme product, as well as the detachment of phase-transitioned lysozyme nanofilm (PTLF) from a substrate surface under the stimulus of Vc solution. As the first case of PTLF coatings in clinical application, we fabricated a novel wound dressing, PTLF@gauze, by simply immersing pristine gauze in the phase-transitioned lysozyme aqueous solution under room temperature. The PTLF@gauze as a dressing could improve wound healing owing to the anti-infection properties of PTLF, and also showed less cell adhesion and required less peeling strength than the pristine gauze due to the disassembly and detachment of PTLF in Vc solution. This stimulus-responsive proteinaceous wound dressing exhibits great potential in clinical application through reducing secondary trauma and relieving patients pain. We expect that this work may drive a universal, low-cost and scalable strategy to form a smart biofunctional surface and open a new avenue for advanced biomaterials.

### 4. Experimental

#### Materials and animals

Lysozyme, tris(2-carboxyethyl)phosphine (TCEP), vitamin C, Thioflavin-T (ThT), 8-anilino-1-naphthalenesulfonic acid (ANS) and BSA-FITC were purchased from Sigma-Aldrich. Ultrapure water was used in all experiments and was supplied by Milli-Q Advantage A10 (Millipore, USA). The Si wafer was purchased from Resemi Co., Ltd, and was cleaned with Piranha solution (concentrated  $\text{H}_2\text{SO}_4$ :35%  $\text{H}_2\text{O}_2$  = 7:3 v/v) at 80 °C for 8 hours before use. An Au (45 nm Au with 5 nm Cr as the adhesion promotion layer) wafer was prepared by magnetron sputtering deposition on cleaned Si wafer. Dialysis membranes (*W*. 34 mm, Diam. 22 mm and Vol. 3.7 mL  $\text{cm}^{-1}$ , Mwco. 2000 D) were purchased from X' A LUOSENBO Tech. Co., Ltd. The sterile gauze was purchased from a drugstore. C57BL/6 mice (male, 18–20 g) were purchased from the Experimental Animal Department of the Army Medical University. All of the animals were used in accordance with ethical standards, the animal protocols were approved by the Institutional Animal Care and Use Committee of the Army Medical University, and all animal experiments followed the Regulation on the Management of Laboratory Animals, which was issued by the Chinese Association for Laboratory Animal Sciences (CALAS). The animals were individually raised in plastic cages under standardized conditions (room temperature: 25 °C; relative humidity: 50%; and circadian rhythm: 12 hours). The animals were fed autoclaved standard rodent chow and water *ad libitum* and were adaptively bred for 1 week in the facility before the experiments.

#### Characterizations

Fluorescence spectra were collected using an F-7000 fluorescence spectrophotometer (Hitachi, Japan). The ATR-FTIR was

collected using a Frontier FT-IR spectrometer (PE, USA). Far-UV CD spectra were obtained using a chirascan spectrophotometer (Applied Photophysics Ltd, England). For Transmission Electron Microscopy (TEM) analysis, a JEM-2100 (JEOL, Japan) transmission microscope with an acceleration voltage of 120 kV was utilized. Field Emission Scanning Electron Microscope (FE-SEM) observations were conducted on a SU8020 (Hitachi, Japan) with an acceleration voltage of 1 kV and all the samples were without gold coating. Energy Dispersive X-Ray Spectroscopy (EDS) was performed on a FEI Quanta 200 with an acceleration voltage of 20 kV and the samples were used with gold coating. Atomic Force Microscopy (AFM) was performed by a Dimension Icon AFM (Bruker) in ScanAsyst mode. The thickness of the phase-transitioned lysozyme nanofilm (PTLF) on a substrate was measured using spectroscopic ellipsometry (Ellip-SR-II, China). SDS-PAGE was performed in tricine buffer (pH 8.45) using an 8% stacking gel and a 16.5% separating gel. The bands of the gel were visualized using Coomassie brilliant blue R-250 staining. X-ray photoelectron spectroscopy (XPS) was performed with a AXIS ULTRA from Kratos Analytical Co., Ltd and the binding energies were calibrated by setting the C1s peak at 284.5 eV. Laser confocal microscopic inspections were conducted using a Leica fluorescence microscope (CTR6000, Leica, Germany). The particle size distribution measurement of colloids was performed using Dynamic light scattering (DLS) on a Malvern Zetasizer Nano-ZS90 (England). Water contact angles (WCA) were measured using an OCA 20 (Dataphysics, Germany). The water vapor transmission rate (WVTR) was measured on a W3/031 water vapor transmission rate tester (Labthink, China) (humidity, 90% RH; temperature, 37 °C). The water uptake was measured by a gravimetric method (temperature, 37 °C).

#### The preparation of the phase-transitioned lysozyme (PTL) product

In order to obtain the phase-transitioned lysozyme (PTL), phase transition lysozyme aqueous solution was freshly prepared by mixing lysozyme solution (2 mg  $\text{mL}^{-1}$ ) with TCEP solution (50 mM, pH 7.2) at the volume ratio of 1:1. The phase transition of the lysozyme was initiated spontaneously upon mixing, and the PTL product in the form of a 2D nanofilm (PTLF) at the solution surface and a network consisting of microparticle-aggregated necklace-like fibers in the bulk solution were achieved in a few minutes.

#### The formation of PTLF on the substrate surface *via in situ* immersion

Simple immersion is enough to transfer efficiently the PTLF onto the immersed target substrate surface to form a solid-supported nanofilm. In this way, the clean Si or Au wafer or gauze was directly immersed into the freshly prepared phase transition aqueous solution (a mixture of 2 mg  $\text{mL}^{-1}$  lysozyme solution and 50 mM, pH 6.2 or 7.2 TCEP solution at the volume ratio of 1:1), and after incubating for 60 minutes, a conformal PTLF was stably attached onto the immersed solid surface. The coated substrate was then taken out and rinsed with ultrapure

water to wash away remaining native lysozymes and other salts. The coated substrate was then subjected to use after N<sub>2</sub> gas drying.

### Far-UV circular dichroism (CD) assay

Due to the requirement of the sample concentration for the far-UV CD spectrum, 50  $\mu\text{L}$  of native lysozyme solution (1 mg mL<sup>-1</sup>), PTL product solution (lysozyme: 1 mg mL<sup>-1</sup>, TCEP: 50 mM, pH 7.2), or PTL product solution incubated with vitamin C (lysozyme: 1 mg mL<sup>-1</sup>, TCEP: 50 mM, pH 7.2, vitamin C: 10 mM) was diluted with 2 mL ultrapure water. Far-UV CD spectra were then collected under a constant nitrogen flush at 25 °C, and recorded from 190 nm to 260 nm with a 2.0 nm bandwidth. All of the data were treated with a baseline correction and the signal of molecularly dissolved vitamin C was subtracted.

### Thioflavin T (ThT) staining

250  $\mu\text{L}$  ThT solution (1 mM) was mixed with 750  $\mu\text{L}$  freshly prepared lysozyme (2 mg mL<sup>-1</sup>) and incubated for 60 minutes in a cuvette in the dark. Then 1 mL TCEP solution (50 mM, pH 7.2) was added to the cuvette and the stained samples were measured by a fluorescence spectrophotometer with excitation at 440 nm and emission at 484 nm. The bandwidths of the excitation and emission slits were set as 5 nm. When there was no change in fluorescence intensity, 2 mL vitamin C solution (250 mM) was added to the cuvette, and the fluorescence spectra were collected with time.

### 8-Anilino-1-naphthalenesulfonic acid (ANS) staining

250  $\mu\text{L}$  ThT solution (1 mM) was mixed with 750  $\mu\text{L}$  freshly prepared lysozyme (2 mg mL<sup>-1</sup>) and incubated for 60 minutes in a cuvette in the dark. Then 1 mL TCEP solution (50 mM, pH 7.2) was added to the cuvette and the stained samples were measured by a fluorescence spectrophotometer with excitation at 355 nm and emission at 470 nm. The bandwidths of the excitation and emission slits were set as 5 nm. When there was no change in fluorescence intensity, 2 mL vitamin C solution (250 mM) was added to the cuvette, and the fluorescence spectra were collected with time.

### Transmission electron microscopy (TEM)

1 mL lysozyme solution (2 mg mL<sup>-1</sup>) and 1 mL TCEP solution (50 mM, pH 7.2) were reacted at room temperature for 1 hour, and then incubated with an equal volume of 250 mM vitamin C solution. The mixture was dialyzed for 24 hours to remove residual vitamin C. Then, 100  $\mu\text{L}$  of this solution was taken out and diluted to 5 mL. A copper grid (supported by carbon film) was immersed into the diluted sample and taken out after 5 seconds. The liquid drop was absorbed by a filter paper immediately and further negatively stained with 0.5–2% (w/v) phosphotungstic acid aqueous solution (pH 7.0) for about 5 minutes.

### Protein release assays

The adhesion and release of proteins were assessed using BSA-FITC solution (10  $\mu\text{L}$  mL<sup>-1</sup> in PBS, pH = 7.4). In brief, the samples were incubated in BSA-FITC solution at 4 °C for 12 h. They were then gently rinsed with ultrapure water to

remove loosely attached protein and buffer salts. For protein release, the surfaces with adherent BSA-FITC were immersed in a 250 mM vitamin C solution for 20 minutes and then rinsed with ultrapure water. The fluorescence intensity of the BSA-FITC remaining attached to the surfaces was determined using an F-7000 fluorescence spectrophotometer.

### Bacterial release assays

Red fluorescent *E. coli*, DH5 $\alpha$ -pBADDs Red, provided by Dr Ruiqing Yan, an affiliate to the Institute of Biophysics, Chinese Academy of Science, was used in this experiment. The adhesion and release of bacteria were assessed using an *E. coli* suspension (1  $\times$  10<sup>7</sup> colony forming units (CFU) mL<sup>-1</sup> in PBS, pH = 7.4). In brief, the samples were incubated in 500  $\mu\text{L}$  of the suspension at 37 °C for 1 h without stirring. They were then gently rinsed with sterile water to remove loosely attached bacteria and buffer salts. For bacterial release, the surfaces with adherent bacteria were immersed in a sterile 250 mM vitamin C solution for 20 minutes and then rinsed with sterile water. The number of bacteria remaining attached to the surfaces was determined using a Leica fluorescence microscope (CTR6000, Leica, Germany), and images of 15 randomly chosen fields were captured. Three replicates were examined, and the density of adherent bacteria was determined using Image-Pro Plus 6.0 (IPP 6.0) software.

### Cell release assays

Typically, the pristine Au wafer and PTLF coated Au wafer were sterilized using 75% ethanol three times, then rinsed with PBS buffer. The samples were put in a 48-well plate, and L929 cells at a density of 5000 cells per well were seeded onto the samples and incubated for 12 hours to allow full cell attachment at 37 °C in a humidified atmosphere with 5% CO<sub>2</sub>. After 12 hours incubation, 250 mM vitamin C solution was added into the cell medium and the cells were incubated in this medium for another 20 minutes. The cells adhered on the samples were stained with calcein and were photographed using a Leica fluorescence microscope (CTR6000, Leica, Germany). The number of cells was counted using Image-Pro Plus 6.0 (IPP 6.0) software.

### Cytotoxicity evaluation of the PTLF@gauze

GFP transgenic fibroblasts were isolated from GFP transgenic neonatal mice as previously described.<sup>56</sup> The 3rd-passage sub-cultured fibroblasts were used for the following experiment. The pristine gauze and PTLF@gauze were cut into discs with a diameter of 0.4 cm using a punch, and placed into the bottom of each well of a 96-well plate. Fibroblast suspension was adjusted to 1  $\times$  10<sup>4</sup> mL<sup>-1</sup> and 100  $\mu\text{L}$  of the cell suspension was seeded on each sample. Cells cultured in the well without a sample served as controls. After incubation at 37 °C in 5% CO<sub>2</sub> incubator for 3 days, the morphology of the fibroblasts on the surface of samples was observed using a fluorescence microscope (Olympus, Japan). The number of cells on the samples was also counted using a Cell Counting Kit-8 (CCK8; Dojindo, Japan). After incubation for 3 days, samples were placed into a new 96-well culture plate containing 100 mL DMEM culture medium in each well. Then, 10 mL of CCK8 was added to each

well. After incubation at 37 °C for 2 h, the absorbance was measured at 450 nm using an enzyme-linked immunosorbent assay reader (Thermo Varioskan Flash, USA).

### Strength test

To examine the strength required when the dressing was removed from the wound, a strength test was performed. Briefly, C57BL/6 mice were under anesthesia with 1% pentobarbital *via* an intraperitoneal injection. A 10 mm × 10 mm full-thickness defect wound was prepared by excision on the back of the mouse, and then the gauze or PTLF modified gauze (PTLF@gauze) was sutured and dressed on the wound. The dressing was removed at day 1 or day 3, and the dressing was soaked with ultrapure water or 500 mM vitamin C solution for one minute before removing. The strength required to remove the dressing from the wound was measured with a spring balance scale. The measurements were repeated 8 times ( $n = 8$ ).

### Cell adhesion test

As mentioned above, the wounds were created, the dressings (gauze or PTLF@gauze) were applied on to the wounds, and the dressings were removed from the wounds after soaking with ultrapure water or 500 mM vitamin C solution at day 1 or day 3. The cells adhered on to the dressings were stained with 4',6-diamidino-2-phenylindole (DAPI) and were photographed using a Leica fluorescence microscope (CTR6000, Leica, Germany). The number of cells was counted using Image-Pro Plus 6.0 (IPP 6.0) software.

### *In vivo* anti-infection and wound healing experiment

The *in vivo* anti-infection and wound healing experiments were performed as previously reported with minor revisions.<sup>57</sup> A two-wound model was created using a sterile biopsy punch, with a diameter of each wound of 0.4 cm.<sup>58</sup> Then, a bacterial suspension of *E. coli* was adjusted to  $10^9$  CFU mL<sup>-1</sup>, and 10 μL suspension was dropped on each wound. The gauze or PTLF@gauze was then dressed and fixed on the wound using an adhesive membrane (NPWT-1, Negative pressure wound therapy kit, China),<sup>59</sup> and for the control group, the wound was covered with the adhesive membrane directly. On day 0, day 1, day 3 and day 7 post-surgery, the wounds were photographed and the dressings were changed. The areas of the wounds were measured using Image Pro Plus 6.0 software. Meanwhile, the wound exudation was collected and the number of bacteria in the exudation at day 1 and day 3 was determined by routine CFU analysis on an agar dish with different dilutions. At day 7 post-surgery, the wound tissues were carefully biopsied, fixed with 4% formaldehyde, embedded in paraffin, sectioned at a thickness of 5 mm and stained with H&E for histological observation. The expression of CD206 and CCR7 in the wound tissue was detected using immunohistochemical staining in the same way as previously reported.<sup>60</sup> The paraffin sections were deparaffinized and rehydrated. After heat-mediated antigen retrieval in citrate buffer, the sections were incubated with 3% H<sub>2</sub>O<sub>2</sub>, blocked with 10% normal goat serum and incubated with a primary antibody (anti-CD206 antibody, 1:800 dilution,

Abcam; anti-CCR7 antibody, 1:800 dilution, Abcam) overnight at 4 °C. The sections were incubated with biotinylated goat anti-rabbit IgG antibody (Zhongshan Biology Company, China), sequentially incubated with an avidin peroxidase reagent (Zhongshan Biology Company) and a diaminobenzidine solution (Zhongshan Biology Company). Ultimately the sections were counterstained with haematoxylin and photographed using an optical microscope (CTR6000, Leica).

## Conflicts of interest

There are no conflicts to declare.

## Acknowledgements

J. Z. and Y. Q. contributed equally to this work. P. Y. appreciates the funding from the National Natural Science Foundation of China (no. 51673112), the 111 Project (no. B14041), the Fundamental Research Funds For the Central Universities (GK201801003, 2017CSZ004) and the Open Project of the State Key Laboratory of Supramolecular Structure and Materials (no. sklssm201827). J. Z. acknowledges the General Financial Grant from the China Postdoctoral Science Foundation (no. 2017M623109). Q. Y. acknowledges the National Natural Science Foundation of China (no. 21774086, 21334004) and the National Key Research and Development Program of China (2016YFC1100402). R. X. acknowledges the Miao Pu project of the Army Medical University (no. 2017R016).

## References

- 1 R. Xu, G. X. Luo, H. S. Xia, W. F. He, J. Zhao, B. Liu, J. L. Tan, J. Y. Zhou, D. S. Liu, Y. Z. Wang, Z. H. Yao, R. X. Zhan, S. S. Yang and J. Wu, *Biomaterials*, 2015, **40**, 1.
- 2 G. D. Mogosanu and A. M. Grumezescu, *Int. J. Pharm.*, 2014, **463**, 127.
- 3 Z. J. Fan, B. Liu, J. Q. Wang, S. Y. Zhang, Q. Q. Lin, P. W. Gong, L. M. Ma and S. R. Yang, *Adv. Funct. Mater.*, 2014, **24**, 3933.
- 4 N. M. Lee, C. Erisken, T. Iskratsch, M. Sheetz, W. N. Levine and H. H. Lu, *Biomaterials*, 2017, **112**, 303.
- 5 A. Meftahi, R. Khajavi, A. Rashidi, M. Sattari, M. Yazdanshenas and M. Torabi, *Cellulose*, 2010, **17**, 199.
- 6 J. P. Chen, C. Y. Kuo and W. L. Lee, *Appl. Surf. Sci.*, 2012, **262**, 95.
- 7 C. Dhand, M. Venkatesh, V. A. Barathi, S. Harini, S. Bairagi, E. Goh Tze Leng, N. Muruganandham, K. Z. W. Low, M. H. U. T. Fazil, X. J. Loh, D. K. Srinivasan, S. P. Liu, R. W. Beuerman, N. K. Verma, S. Ramakrishna and R. Lakshminarayanan, *Biomaterials*, 2017, **138**, 153.
- 8 A. McLister, J. McHugh, J. Cundell and J. Davis, *Adv. Mater.*, 2016, **28**, 5732.
- 9 K. T. Huang, Y. L. Fang, P. S. Hsieh, C. C. Li, N. T. Dai and C. J. Huang, *J. Mater. Chem. B*, 2016, **4**, 4206.

- 10 A. G. Nejad, C. H. Park and C. S. Kim, *Biomacromolecules*, 2016, **17**, 1213.
- 11 L. Mi, H. Xue, Y. T. Li and S. Y. Jiang, *Adv. Funct. Mater.*, 2011, **21**, 4028.
- 12 L. Mi and S. Y. Jiang, *Angew. Chem., Int. Ed.*, 2014, **53**, 1746.
- 13 S. Tanodekaewa, M. Prasitsilp, S. Swasdison, B. Thavornuyutikarn, T. Pothsree and R. Pateepasen, *Biomaterials*, 2004, **25**, 1453.
- 14 A. R. Unnithan, A. G. Nejad, A. R. K. Sasikala, R. G. Thomas, Y. Y. Jeong, P. Murugesan, S. Nasser, D. M. Wu, C. H. Park and C. S. Kim, *Chem. Eng. J.*, 2016, **287**, 640.
- 15 K. W. Kolewe, K. M. Dobosz, K. A. Rieger, C. C. Chang, T. Emrick and J. D. Schiffman, *ACS Appl. Mater. Interfaces*, 2016, **8**, 27585.
- 16 S. N. Pour, S. V. Ghugare, R. Wiens, K. Gough and S. Liu, *Appl. Surf. Sci.*, 2015, **349**, 695.
- 17 K. K. Ou, X. J. Wu, B. X. Wang, C. Meng, X. Dong and J. X. He, *Cellulose*, 2017, **24**, 5211.
- 18 I. Cherny and E. Gazit, *Angew. Chem., Int. Ed.*, 2008, **47**, 4062.
- 19 D. Li, E. M. Jones, M. R. Sawaya, H. Furukawa, F. Luo, M. Ivanova, S. A. Sievers, W. Y. Wang, O. M. Yaghi, C. Liu and D. S. Eisenberg, *J. Am. Chem. Soc.*, 2014, **136**, 18044.
- 20 T. P. J. Knowles and R. Mezzenga, *Adv. Mater.*, 2016, **28**, 6546.
- 21 C. Li, R. R. Qin, R. R. Liu, S. T. Miao and P. Yang, *Biomater. Sci.*, 2018, **6**, 462.
- 22 P. Yang, *Macromol. Biosci.*, 2012, **12**, 1053.
- 23 A. Gao, Q. Wu, D. Wang, Y. Ha, Z. Chen and P. Yang, *Adv. Mater.*, 2016, **28**, 579.
- 24 D. Wang, Y. Ha, J. Gu, Q. Li, L. Zhang and P. Yang, *Adv. Mater.*, 2016, **28**, 7414.
- 25 D. Wang, Z. Wu, A. Gao, W. Zhang, C. Kang, Q. Tao and P. Yang, *Soft Matter*, 2015, **11**, 3094.
- 26 Y. Ha, J. Yang, F. Tao, Q. Wu, Y. Song, H. Wang, X. Zhang and P. Yang, *Adv. Funct. Mater.*, 2018, **28**, 1704476.
- 27 J. Gu, Y. J. Su, P. Liu, P. Li and P. Yang, *ACS Appl. Mater. Interfaces*, 2017, **9**, 198.
- 28 D. Eisenberg and M. Jucker, *Cell*, 2012, **48**, 1188.
- 29 G. L. Bowman, *BioFactors*, 2012, **38**, 114.
- 30 K. Murakamia, N. Murataa, Y. Ozawa, N. Kinoshita, K. Irie, T. Shirasawa and T. Shimizu, *J. Alzheimer's Dis.*, 2011, **26**, 7.
- 31 F. E. Harrison, *J. Alzheimer's Dis.*, 2012, **29**, 711.
- 32 M. Ravid, B. Chen, J. Bernheim and I. Kedar, *Br. J. Exp. Pathol.*, 1985, **66**, 137.
- 33 Y. H. Lien, J. H. Wu, J. W. Liao and T. M. Wu, *Macromol. Res.*, 2013, **21**, 511.
- 34 W. Lee, I. Kim, S. W. Lee, H. Lee, G. Lee, S. Kim, S. W. Lee and D. S. Yoon, *Macromol. Res.*, 2016, **24**, 868.
- 35 C. Li, L. Xu, Y. Zuo and P. Yang, *Biomater. Sci.*, 2018, **6**, 836.
- 36 J. Gu, S. Miao, Z. Yan and P. Yang, *Colloid Interface Sci. Commun.*, 2018, **22**, 42.
- 37 Y. Qu, T. Wei, J. Zhao, S. Jiang, P. Yang, Q. Yu and H. Chen, *J. Mater. Chem. B*, 2018, **6**, 3946.
- 38 N. J. Greenfield, *Nat. Protoc.*, 2006, **1**, 2876.
- 39 M. Biancalana and S. Koide, *Biochim. Biophys. Acta*, 2010, **1804**, 1405.
- 40 A. Moro, C. Gatti and N. Delorenzi, *J. Agric. Food Chem.*, 2001, **49**, 4784.
- 41 J. P. Yuan and F. Chen, *J. Agric. Food Chem.*, 1998, **46**, 5078.
- 42 C. Q. He, Y. B. Hou, Y. C. Han and Y. L. Wang, *Langmuir*, 2011, **27**, 4551.
- 43 J. N. Abraham, D. Kedracki, E. Prado, C. Gourmel, P. Maroni and C. Nardin, *Biomacromolecules*, 2014, **15**, 3253.
- 44 P. A. Rühls, J. Adamcik, S. Bolisetty, A. Sanchez-Ferrer and R. Mezzenga, *Soft Matter*, 2011, **7**, 3571.
- 45 Y. Porat, A. Abramowitz and E. Gazit, *Chem. Biol. Drug Des.*, 2006, **67**, 27.
- 46 L. Bi and G. Pan, *J. Mater. Chem. A*, 2014, **2**, 3715.
- 47 Q. Yu, J. Cho, P. Shivapooja, L. K. Ista and G. P. Lopez, *ACS Appl. Mater. Interfaces*, 2013, **5**, 9295.
- 48 T. Wei, Z. Tang, Q. Yu and H. Chen, *ACS Appl. Mater. Interfaces*, 2017, **9**, 37511.
- 49 Y. Qu, T. Wei, W. Zhan, C. Hu, L. Cao, Q. Yu and H. Chen, *J. Mater. Chem. B*, 2017, **5**, 444.
- 50 S. A. Eming, P. Martin and M. Tomic-Canic, *Sci. Transl. Med.*, 2014, **6**, 265.
- 51 R. Edwards and K. G. Harding, *Curr. Opin. Infect. Dis.*, 2004, **17**, 91.
- 52 V. Nizet, T. Ohtake, X. Lauth, J. Trowbridge, J. Rudisill, R. A. Dorschner, V. Pestonjamas, J. Piraino, K. Huttner and R. L. Gallo, *Nature*, 2001, **414**, 454.
- 53 X. Zhao, H. Wu, B. L. Guo, R. N. Dong, Y. S. Qiu and P. X. Ma, *Biomaterials*, 2017, **122**, 34.
- 54 N. Annabi, D. Rana, E. S. Sani, R. Portillo-Lara, J. L. Gifford, M. M. Fares, S. M. Mithieux and A. S. Weiss, *Biomaterials*, 2017, **139**, 229.
- 55 W. Y. Chen, H. Y. Chang, J. K. Lu, Y. C. Huang, S. G. Harroun, Y. T. Tseng, Y. J. Li, C. C. Huang and H. T. Chang, *Adv. Funct. Mater.*, 2015, **25**, 7189.
- 56 B. Cheng, H. W. Liu, X. B. Fu, Z. Y. Sheng and J. F. Li, *Br. J. Dermatol.*, 2008, **158**, 713.
- 57 M. Y. El-Naggar, Y. M. Gohar, M. A. Sorour and M. G. Waheeb, *J. Microbiol. Biotechnol.*, 2016, **26**, 408.
- 58 X. R. Zhang, R. Xu, X. H. Hu, G. X. Luo, J. Wu and W. F. He, *Burn Trauma*, 2015, **3**, 15.
- 59 Z. H. Yao, Y. Huang, G. X. Luo, J. Wu and W. F. He, *Burn Trauma*, 2014, **2**, 196.
- 60 R. Xu, Y. Bai, J. Zhao, H. S. Xia, Y. Kong, Z. H. Yao, R. S. Yan, X. R. Zhang, X. H. Hu, M. X. Liu, Q. W. Yang, G. X. Luo and J. Wu, *J. Tissue Eng. Regen. Med.*, 2018, **12**, 905.